

A theoretical study of the inland trough of northeastern Australia

M. Adams, National Meteorological Centre, Melbourne, Australia

(Manuscript received August 1984; revised August 1986)

A two-layer, quasi-geostrophic model incorporating orography, surface heating and the release of latent heat in convection is used to study the semi-permanent trough/ridge system of northeastern Australia. The model produces realistic flow patterns and these are used to examine the way in which various parameters affect the flow. It is found that the factors which are most favourable for a large-amplitude trough/ridge system are: (a) a shallow easterly low-level airstream, and (b) weak vertical wind shear.

Results obtained suggest that there may be a positive feedback between latent heat released and the inland trough acting in such a way that the trough triggers the release of latent heat which, in turn, assists in maintaining the trough.

Introduction

The most commonly observed surface synoptic chart of northeastern Australia shows a ridge in the prevailing southeasterly winds close to the east coast of Queensland, and a trough inland. This pattern occurs throughout the whole year, but more frequently in summer, though there are innumerable variations in the strength and position of the trough/ridge system. The inland trough is a major feature of the synoptic-scale circulation often extending southwards into New South Wales and occasionally into Victoria as well. It varies in longitudinal position according to the meteorological situation; being pushed westwards when there is ridging on Queensland's east coast or in the Coral Sea, and moving to the east when a high pressure system is establishing itself over the continent of Australia or in the Great Australian Bight. Under the former set of circumstances the trough may move out of Queensland into the Northern Territory and South Australia.

Apart from the effects of synoptic-scale forcing, there are two diurnal variations of the inland trough. Firstly, during the afternoons (particularly in the hotter months), a marked deepening of the trough takes place. Secondly, the trough very often moves to the east in the afternoons and to the west at night. The first effect demonstrates that there is a strong correlation between the intensity of the trough and the amount of surface heating. This obvious relationship is responsible for the trough often being referred to as a heat trough. The second effect is linked to the dry line properties of the inland trough. The trough almost always defines the demarcation between relatively moist air to the east and much drier air to the west. Surface heating gives rise to mixing in the lower troposphere which dries the surface layer of air. The

dry line and trough, therefore, move towards the Queensland coast in the afternoons. In summer the deepening of the trough and its movement provide a sufficient trigger for showers and thunderstorms. These showers and storms usually form on and just east of the trough. Sometimes the whole air mass east of the trough is moist and unstable enough for convective activity. On other occasions this activity is confined to a narrow region adjacent to the trough. If the atmosphere is too stable for showers or storms, as is generally the case in winter, afternoon cumulus clouds still form over the land mass on the eastern flank of the trough.

As the inland trough is not uncommon in winter, it is clear that intense solar insolation is not the only causative mechanism involved. Arguments based on the conservation of potential vorticity show that there is a contribution to the production of a trough/ridge system from the Great Dividing Range. The influence of mountains on low-level easterly air flow is felt in upstream perturbations of the flow and leads to a ridge along the mountain range and a lee trough (e.g. Wiin-Nielsen 1973).

Although the trough/ridge combination is the most prominent meteorological feature of northeastern Australia, very little theoretical work has been carried out to explain and examine the trough. The only studies directly related to it are those of De Lisle and Harper (1961) (using a model by Smagorinsky 1953) and Fandry and Leslie (1984). In addition, Leslie (1980) and Skinner and Leslie (1982) have shown that the incorporation of a properly constituted surface heat budget equation into the Australian Region Primitive Equation model (ARPE) will result in a summer heat trough and low over the continent.

De Lisle and Harper (1961) determined that in the absence of complicating effects due to orography, a surface trough is formed which is displaced from the position of maximum heating. Fandry and Leslie's (1984) model consists of a two-layer, quasi-geostrophic scheme subject to perturbations arising from orography and surface heating. In their analysis it is assumed that the damp southeasterly trade winds drop their moisture as they cross the coastline; the two atmospheric layers are supposed to be well mixed so that each layer has a constant potential temperature; and the mountains are parameterised with a ninety degree slope on their eastern side. This model was able to simulate well-developed troughs in the region of strongest surface heating.

In the present paper the trough is investigated by means of a two-layer baroclinic model similar to that of Derome and Wiin-Nielsen (1971). Realistic orography, surface heating and latent heat release by convective clouds are included in the model's formulation.

Formulation of the equations

The atmosphere, depth 1000 hPa, is divided into two layers as shown in Fig. 1. Each layer is subdivided into two equal parts by pressure. The steady-state, quasi-geostrophic vorticity and thermodynamic equations with pressure as the vertical coordinate form the basis of the model. These equations are, respectively,

$$\underline{V} \cdot \nabla(\zeta + f) = (\zeta + f) \partial \omega / \partial p \quad \dots 1$$

and

$$\underline{V} \cdot \nabla(\partial \phi / \partial p) + \sigma \omega = -RQ/pC_p \quad \dots 2$$

where \underline{V} is the horizontal velocity vector, ζ is the vorticity, f is the Coriolis parameter, ω is the vertical velocity in pressure coordinates, ϕ is the geopotential height, σ is the static stability parameter ($-\alpha \partial(\ln \theta) / \partial p$), R is the gas constant, p is the pressure, C_p is the specific heat of dry air at constant pressure, Q is the diabatic heat per unit mass per unit time, and ∇ is the gradient operator in two dimensions.

The vorticity equation is applied at levels 1 and 3 (the standard levels). Assuming the vertical velocity at the top of the atmosphere is zero, we have

$$\underline{V}_1 \cdot \nabla(\zeta_1 + f) = (\zeta_1 + f) \omega_2 / 2P_1 \quad \dots 3$$

and

$$\underline{V}_3 \cdot \nabla(\zeta_3 + f) = (\zeta_3 + f) (\omega_4 - \omega_2) / 2P_3 \quad \dots 4$$

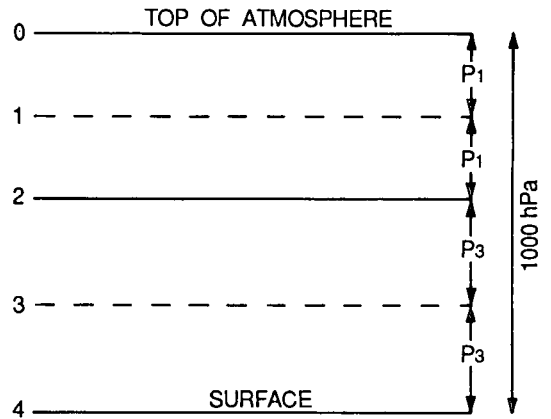
where $2P_1$ is the pressure depth of the upper layer and $2P_3$ is the pressure depth of the lower layer. The subscripts 0 to 4 refer to values of variables at levels 0 to 4 as shown in Fig. 1.

The thermodynamic equation at level 2 gives

$$\frac{1}{P} [\underline{V}_2 \cdot \nabla(\phi_3 - \phi_1)] + \sigma_2 \omega_2 = -RQ_2 / 2P_1 C_p \quad \dots 5$$

where $P = P_1 + P_3 = 500$ hPa.

• Fig. 1 Vertical layering of the atmosphere used in the formulation of the model.



We assume a linear variation of the velocity vector with pressure between standard levels so that

$$\underline{V}_2 = (P_1 \underline{V}_3 + P_3 \underline{V}_1) / P \quad \dots 6$$

$$\underline{V}_4 = [(P + P_3) \underline{V}_3 - P_3 \underline{V}_1] / P \quad \text{and} \quad \dots 7$$

$$\phi_4 = [(P + P_3) \phi_3 - P_3 \phi_1] / P \quad \dots 8$$

The value of ω at the lower boundary may be evaluated from

$$\omega_4 = \underline{V}_4 \cdot \nabla p_t - \rho_4 g C_D \zeta_4 / f \quad \dots 9$$

where p_t is the pressure at the lower boundary, ρ is the density, g is the acceleration due to gravity, and C_D is the drag coefficient. This equation is derived by assuming a steady state and using the condition of the vertical velocity in height coordinates at the lower boundary being proportional to the planetary boundary layer vorticity ζ_4 (see e.g. Wiin-Nielsen 1973).

Elimination of ω_2 and ω_4 gives

$$\underline{V}_1 \cdot \nabla(\zeta_1 + f) + \frac{(\zeta_1 + f) (P_1 \underline{V}_3 + P_3 \underline{V}_1) \cdot \nabla(\phi_3 - \phi_1)}{2P_1 P^2 \sigma_2} - \frac{(\zeta_1 + f) RQ_2}{4P_1^2 C_p \sigma_2} \quad \dots 10$$

and

$$\underline{V}_3 \cdot \nabla(\zeta_3 + f) + \frac{(\zeta_3 + f) \rho_4 g C_D \zeta_4}{2P_3 f} - \frac{(\zeta_3 + f) (P_1 \underline{V}_3 + P_3 \underline{V}_1) \cdot \nabla(\phi_3 - \phi_1)}{2P^2 P_3 \sigma_2} = \quad \dots 11$$

$$\frac{(\zeta_3 + f) [(P + P_3) \underline{V}_3 - P_3 \underline{V}_1] \cdot \nabla p_t}{2P_3 P} + \frac{(\zeta_3 + f) RQ_2}{4P_1 P_3 C_p \sigma_2}$$

To linearise Eqns 10 and 11 we assume

$$\phi_1 = -U_1 y (f - \beta y / 2) + \phi'_1 \quad \dots 12$$

$$\phi_3 = -U_3y(f - \beta y/2) + \phi'_3 \quad \dots 13$$

where U_1, U_3 are constant zonal velocities, $\beta = df/dy$ is also constant and ϕ'_1, ϕ'_3 are perturbation geopotential heights dependent only on the distance x along an east-west axis. The y -axis lies in a meridional direction. The assumption that ϕ'_1 and ϕ'_3 are independent of y has the disadvantage of essentially making the model one-dimensional and can only be justified if the perturbation quantities are small. The advantage of the assumption is that the resultant equations become ordinary differential rather than partial differential. Neglecting products of perturbation quantities and using the perfect gas equation gives

$$\frac{U_1}{f} \frac{d^3\phi'_1}{dx^3} + \frac{\beta}{f} \frac{d\phi'_1}{dx} + \frac{f}{2PP_1\sigma_2} \left(\frac{U_1 d\phi'_3}{dx} - \frac{U_3 d\phi'_1}{dx} \right) = -\frac{RQ'_2 f}{4P_1^2 C_p \sigma_2} \quad \dots 14$$

and

$$\begin{aligned} & \frac{U_3}{f} \frac{d^3\phi'_3}{dx^3} + \frac{\beta}{f} \frac{d\phi'_3}{dx} + \frac{gC_D}{P_3 f RT_4} \left[(P + P_3) \frac{d^2\phi'_3}{dx^2} - \frac{P_3 d^2\phi'_1}{dx^2} \right] \\ & - \frac{f}{2P P_3 \sigma_2} \left(\frac{U_1 d\phi'_3}{dx} - \frac{U_3 d\phi'_1}{dx} \right) = \frac{f}{2PP_3} \left[(P + P_3) U_3 - P_3 U_1 \right] \frac{dp_1}{dx} + \frac{fRQ'_2}{4P_1 P_3 C_p \sigma_2} \dots 15 \end{aligned}$$

where Q'_2 is the perturbation value of Q_2 and T_4 is the surface temperature. It has been assumed that p_1 is a function of x only and that dp_1/dx is a perturbation quantity. Equations 14 and 15 may be written

$$\left(\frac{U_1}{f} D^3 + \frac{\beta}{f} D - AU_3 D \right) \phi'_1 = -AU_1 D \phi'_3 + MQ'_2 \quad \dots 16$$

and

$$\begin{aligned} & (JD^2 - BU_3 D) \phi'_3 = \\ & \left(-\frac{U_3}{f} D^3 - HD^2 - \frac{\beta}{f} D - BU_1 D \right) \phi'_3 + \\ & (SU_3 + TU_1) \frac{dp_1}{dx} + NQ'_2 \quad \dots 17 \end{aligned}$$

where $A = f/2PP_1\sigma_2$, $B = -f/2PP_3\sigma_2$, $H = gC_D(P + P_3)/P_3 f RT_4$, $J = -gC_D/fRT_4$, $M = -Rf/4P_1^2 C_p \sigma_2$, $N = Rf/4P_1 P_3 C_p \sigma_2$, $S = f(P + P_3)/2PP_3$, $T = -f/2P$ and $D = d/dx$.

The coupled ordinary differential equations (Eqns 16 and 17) may be uncoupled by acting on Eqn 16 by the operator $JD - BU_3$ and on Eqn 17 by the operator $\frac{U_1 D}{f} + \frac{\beta}{f} - AU_3$. We obtain the linearised equations

$$\mathcal{L}\phi'_3 = (BU_3 - JD)MQ'_2 +$$

$$\left(\frac{U_1 D^2}{f} + \frac{\beta}{f} - AU_3 \right) [(SU_3 + TU_1) \frac{dp_1}{dx} + NQ'_2] \quad \dots 18$$

$$\begin{aligned} \mathcal{L}\phi'_1 &= \left(\frac{U_3 D^2}{f} + HD + \frac{\beta}{f} + BU_1 \right) MQ'_2 \\ & - AU_1 [(SU_3 + TU_1) \frac{dp_1}{dx} + NQ'_2] \quad \dots 19 \end{aligned}$$

where

$$\begin{aligned} \mathcal{L} &= \frac{U_1 U_3 D^5}{f^2} + \frac{HU_1 D^4}{f} + \frac{\beta(U_1 + U_3) D^3}{f} + \\ & \frac{(BU_1^2 - AU_3^2) D^3}{f} + \left(\frac{\beta H}{f} - AHU_3 - JAU_1 \right) D^2 + \\ & \frac{\beta}{f} \left(\frac{\beta}{f} + BU_1 - AU_3 \right) D \quad \dots 20 \end{aligned}$$

The solution to the problem depends on finding functions ϕ'_1 and ϕ'_3 satisfying the linear, inhomogeneous equations 18 and 19.

Solution of the equations

The solution for the functions ϕ'_1 and ϕ'_3 satisfying Eqns 18 and 19 consists of two parts, the general solution and the particular integral. The general solution is determined from the homogeneous equation and describes the baroclinic system without external forcing. We shall only be concerned with the particular integral in this paper since it is produced by the external forcing mechanisms which are the subject of this study.

The method of variation of parameters is used to solve Eqns 18 and 19. Details of this method may be found in most textbooks on the solution of ordinary differential equations (e.g. Burkill 1956). The method involves determining the roots of the characteristic equation

$$\begin{aligned} & \frac{U_1 U_3}{f^2} \mu^5 + \frac{HU_1}{f} \mu^4 + \left[\frac{\beta(U_1 + U_3)}{f^2} + \right. \\ & \left. \frac{(BU_1^2 - AU_3^2)}{f} \right] \mu^3 + \left(\frac{\beta H}{f} - AHU_3 - JAU_1 \right) \mu^2 + \\ & \frac{\beta}{f} \left(\frac{\beta}{f} + BU_1 - AU_3 \right) \mu = 0 \quad \dots 21 \end{aligned}$$

Five values of μ will satisfy this equation for any particular values of the constants. Besides zero, these values turn out to be of the form $\exp(rx)$, $\exp(qx)$, $\exp(\alpha x) \cos(\gamma x)$ and $\exp(\alpha x) \sin(\gamma x)$ where r, q, α and γ are all real and depend on the coefficients of Eqn 21. When calculations are performed in the range of meteorologically plausible values of the coefficients of Eqn 21, α is very small and can conveniently be neglected. (Of all the cases considered, the absolute value of α was never more than 5.7 per cent of the absolute values of r, q and γ .) The particular integral is given by

$$\begin{aligned} \phi'_3 &= f^2 [v_1 + v_2 \exp(rx) + v_3 \exp(qx) + v_4 \cos(\gamma x) \\ & + v_5 \sin(\gamma x)] / U_1 U_3 W \quad \dots 22 \end{aligned}$$

where dv_i/dx ($i=1$ to 5) are found by replacing the i th column in the Wronskian of the system W by the

column $\begin{pmatrix} 0 \\ 0 \\ 0 \\ 0 \\ \text{RHS} \end{pmatrix}$ where RHS is the right-hand side of Eqn 18.

A similar procedure will yield ϕ'_i . The Wronskian itself is given by

$$W = \begin{vmatrix} 1 & 1 & 1 & \cos(\gamma x) & \sin(\gamma x) \\ 0 & r & q^2 & -\gamma \sin(\gamma x) & \gamma \cos(\gamma x) \\ 0 & r^2 & q^2 & -\gamma^2 \cos(\gamma x) & -\gamma^2 \sin(\gamma x) \\ 0 & r^3 & q^3 & \gamma^3 \sin(\gamma x) & -\gamma^3 \cos(\gamma x) \\ 0 & r^4 & q^4 & \gamma^4 \cos(\gamma x) & \gamma^4 \sin(\gamma x) \end{vmatrix} \exp[(r+q)x] \dots 23$$

which simplifies to

$$W = -rq(r-q)(r^2 + \gamma^2)(q^2 + \gamma^2)\gamma^3 \exp[(r+q)x] \dots 24$$

It is also straightforward to evaluate dv_i/dx ($i = 1$ to 5) as functions of RHS. Numerical determination of ϕ_3 and ϕ_1 then depends on choosing appropriate values for the constants and appropriate functions for p_i and Q'_2 .

Numerical solution: orography only

The form of the solution ϕ'_3 is very sensitive to the shape of the terrain since the factor $U_1 D^2(dp_i/dx)/f$ normally dominates RHS. In order to obtain a solution in a closed form we are limited in the choice of functions that can be used to represent dp_i/dx . The function chosen for p_i portrays mountains that rise suddenly from a plain inland and from the sea on their eastern side. The representation is not ideal because of the discontinuities at the base of the mountains. It is considered that this imperfection is compensated for by the ease of integration of the functions dv_i/dx ($i = 1$ to 5).

The function used for orography had the form

$$\begin{aligned} p_i &= k(x > -\delta + \pi/2n) \\ p_i &= 1 + m \cos n(x + \delta) \quad (\pi/2n - \delta \geq x \geq -\pi/2n - \delta) \\ p_i &= k(x < -\pi/2n - \delta) \end{aligned} \dots 25$$

where k, l, m, n and δ are constants.

Using this form for p_i allows explicit solutions for ϕ'_3 and ϕ'_1 to be found. The result for ϕ'_3 is

$$\begin{aligned} \phi'_3 &= \frac{L\{(rq - n^2) \cos n(x + \delta) - n(r + q) \sin n(x + \delta)\}}{a_0(n^2 - \gamma^2)(n^2 + r^2)(n^2 + q^2)} \\ &\left(\frac{\pi}{2n} - \delta \geq x \geq -\frac{\pi}{2n} - \delta\right) \\ \phi'_3 &= 0 \quad \text{otherwise} \end{aligned} \dots 26$$

where $a_0 = U_1 U_3 / f^2$ and $L = m(SU_3 + TU_1)(U_1 n^2 / f - \beta / f + AU_3)$.

To parameterise eastern Australia's orography at 20°S, the actual function (Eqn 25) used was

$$\begin{aligned} p &= 1015 - 100 \cos 4.488x \quad (|x| \leq 0.35) \\ p &= 1015 \quad (|x| \leq 0.35) \end{aligned} \dots 27$$

with x measured in thousands of kilometres from an origin 350 kilometres inland and p_i in hPa. The orography depicted by this equation is shown in Fig. 2.

In the numerical evaluation of ϕ_3 , it was assumed that a low-level easterly wind regime was surmounted by upper-level westerly winds. Altering the values of $U_1 - U_3$ can give some insight into the effect of vertical shear on the flow. It is also of interest to investigate the changes that occur to the flow when the depths of the lower and upper layers are changed. We can, in addition, see how sensitive the flow is to variations in static stability and drag coefficient.

As the flow perturbations induced by orography alone turn out to be rather small, only one case was considered. The values of the constants chosen for this case were: $U_1 = 10 \text{ms}^{-1}$, $U_3 = -10 \text{ms}^{-1}$, $\sigma_2 = 2 \times 10^{-4} \text{m}^3 \text{k}^{-1} (\text{hPa})^{-1}$, $C_D = 2.4 \times 10^{-2} \text{ms}^{-1}$ and $P_3 = 250 \text{hPa}$. These values were considered as the standard ones and called case 1.

The form of the low-level geopotentials for orography alone in the standard situation is shown in Fig. 3. Because of the discontinuities already referred to in the representation of p_i , only the range $|x| \leq 0.35$ is shown.

Numerical solution: orography and surface heating

Surface heating was introduced into the analysis by converting the heating to equivalent orography. The mean daily temperature at 20°S for the summer months (November to February inclusive) varies from

Fig. 2 Orography used in the model.

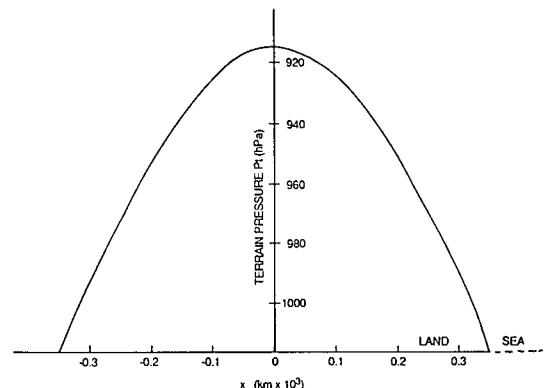
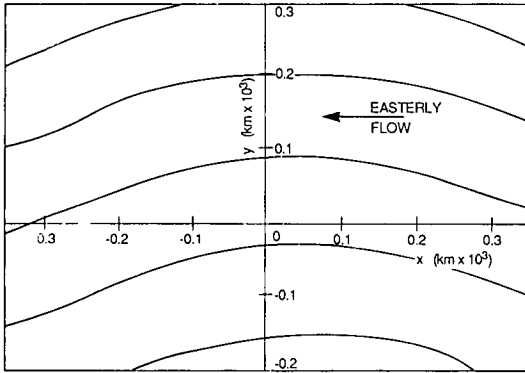


Fig. 3 Lower-layer geopotential pattern for case 1 with orography only (geopotentials at 60 gpm spacing).



27°C, the sea surface temperature, to 31°C about 700 kilometres inland and then remains nearly constant for a considerable distance to the west. The equivalent orography was defined by allowing each degree Celsius above sea surface temperature to represent an orographic depression of 200 metres. The actual value chosen is relatively unimportant since the model's response is primarily to orographic gradients. The function chosen to represent the equivalent orography was

$$P_1 = \begin{matrix} 1015 & (x > 0.35) \\ 1065 - 70.7 \sin 2.244x & (|x| \leq 0.35) \\ 915 & (x < -0.35) \end{matrix} \dots 28$$

where p_1 is the pressure height of the equivalent orography measured in hPa and x is measured in thousands of kilometres.

The total effect of mountains and heating was determined by adding the perturbation induced by Eqn 28 to those of Eqn 26. The perturbations were large enough to test the effect of varying the vertical shear, depth of easterly stream and the mid-troposphere static stability. Seven cases were considered for the lower-layer flow. The parameters used are tabulated below.

Table 1. Values of parameters for the seven flows considered. The value of σ_2 is in units of $10^{-4} \text{m}^3 \text{k}^{-1} (\text{hPa})^{-1}$.

Case number	U_1 (ms^{-1})	U_3 (ms^{-1})	σ_2	P_3 (hPa)
1	10	-10	2	250
2	10	-10	2	150
3	10	-10	2	50
4	10	-10	3	250
5	10	-4	2	250
6	10	-4	2	150
7	20	-20	2	250

In drawing the geopotentials, it is necessary to smooth the curves outside the range $|x| \leq 0.35$ to avoid the large discontinuities that would otherwise arise at $x = 0.35$ and $x = -0.35$. These discontinuities stem from the fact that d^2p/dx^2 and d^3p/dx^3 are not continuous at $x = 0.35$ and $x = -0.35$. It was decided to reduce ϕ'_3 to zero at $x = 0.5$ and $x = -0.5$. It is not difficult to determine cubic forms for ϕ'_3 in the ranges 0.35 to 0.5 and -0.35 to -0.5 that join smoothly to the derived values of ϕ'_3 in the range $|x| \leq 0.35$. These functions are

$$\begin{aligned} \phi'_3 &= k_0 (587.4x^3 - 748.9x^2 + 308.4x - 40.4) & (0.35 \leq x \leq 0.5) \\ \phi'_3 &= -k_1 (587.4x^3 + 748.9x^2 + 308.4x + 40.4) & (-0.35 \geq x \geq -0.5) \end{aligned} \dots 29$$

where k_0 is the value of ϕ'_3 at 0.35 and k_1 is the value of ϕ'_3 at -0.35 , both evaluated from Eqn 26. While this device is artificial, some manipulation of this sort is necessary if the geopotential is to be a smooth function. Because of this artifice, unrealistic patterns in the geopotential field may result in the ranges $0.35 < x < 0.5$ and $-0.35 > x > -0.5$. There is, of course, no distortion of geopotential in the range $|x| \leq 0.35$. The alternative to an equation such as 29 is to use more realistic (and more complex) functions to take account of orography and surface heating. If this were done, functions dv_1/dx to dv_5/dx could not be integrated directly and solutions would have to be found by numerical methods.

The lower-layer geopotentials (ϕ_3) for cases 1 to 7 are shown in Figs 4 to 10 respectively. Figure 11 displays the upper-layer geopotential ϕ_1 for case 1. It was found that the value of the drag coefficient C_D made no appreciable difference to the flow patterns. Also, since the upper-layer perturbations were very small compared to those in the lower layer, only case 1 upper-layer flow was examined.

Fig. 4 Lower-layer geopotential pattern for case 1 with orography and surface heating (geopotentials at 60 gpm spacing).

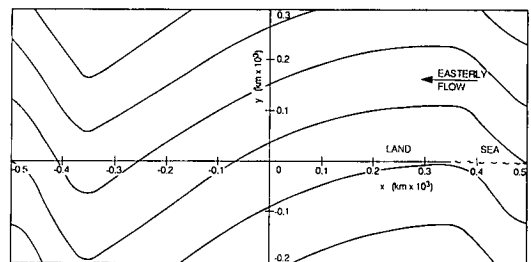


Fig. 5 Lower-layer geopotential pattern for case 2 with orography and surface heating (geopotentials at 60 gpm spacing).

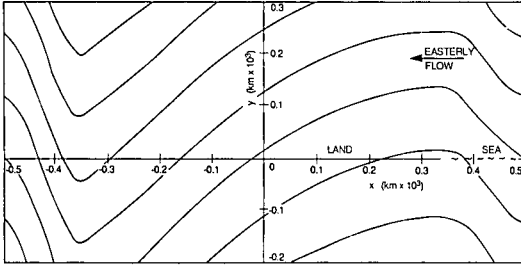


Fig. 6 Lower-layer geopotential pattern for case 3 with orography and surface heating (geopotentials at 120 gpm spacing).

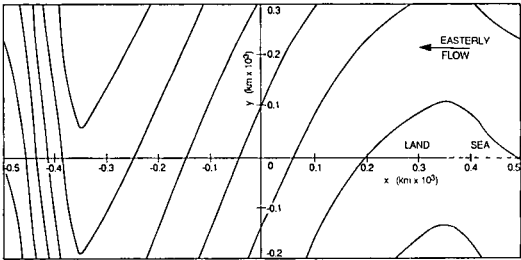


Fig. 7 Lower-layer geopotential pattern for case 4 with orography and surface heating (geopotentials at 60 gpm spacing).

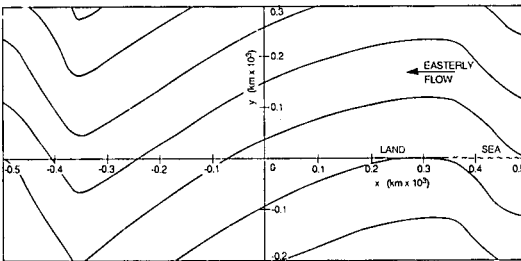


Fig. 8 Lower-layer geopotential pattern for case 5 with orography and surface heating (geopotentials at 30 gpm spacing).

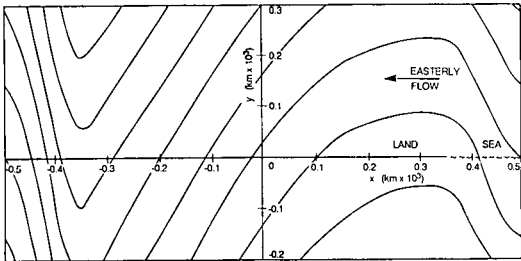


Fig. 9 Lower-layer geopotential pattern for case 6 with orography and surface heating (geopotentials at 30 gpm spacing).

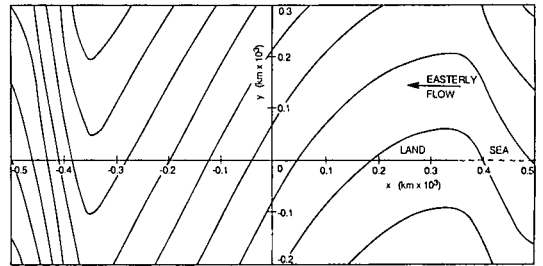


Fig. 10 Lower-layer geopotential pattern for case 7 with orography and surface heating (geopotentials at 120 gpm spacing).

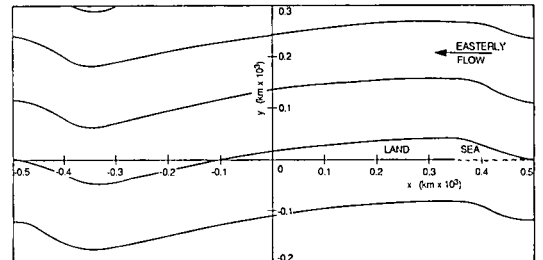
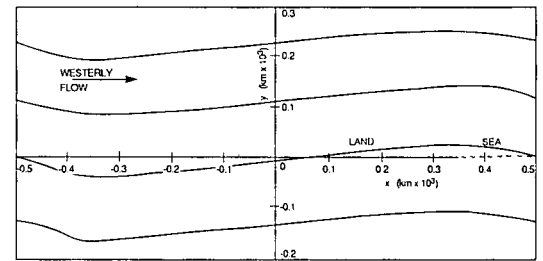


Fig. 11 Upper-layer geopotential pattern for case 1 with orography and surface heating (geopotentials at 60 gpm spacing).



Numerical solution: latent heat release

It has already been noted that the inland trough very often is a dry line and that convective cloud forms east of the trough, particularly on summer afternoons. The latent heat released in the formation of these clouds has, so far, been neglected in modelling the trough. The method of formulation of the present model allows for the introduction of a diabatic heating term Q_2' at level 2. Equation 18 shows that the model's response is not only to the zonal distribution of Q_2' but also to the horizontal variation of dQ_2'/dx and d^2Q_2'/dx^2 . It is by no means obvious how these quantities should

vary. In order to derive even a qualitative measure of the effects of latent heat release, certain assumptions concerning dQ_2/dx and d^2Q_2/dx^2 must be made. The results of this section are based on these assumptions and can, therefore, only be described as tentative.

Satellite photographs show that the demarcation between convective activity east of the trough and generally cloud-free conditions west of the trough is very sharp. Concurrent synoptic observations also point to an abrupt air mass change across the trough line. Therefore it was considered that, as far as adiabatic heating was concerned, the dominant forcing term in Eqn 18 was $-JM dQ_2/dx$, which was large and negative close to the trough, and small elsewhere. This suggested that an appropriate form of the latent heat forcing term would be inversely proportional to the distance east of the trough with the constant of proportionality negative.

Mathematically,

$$Q_2' = \begin{cases} 0 & (x \leq 0) \\ -\Lambda/x & (x > 0) \end{cases} \dots 30$$

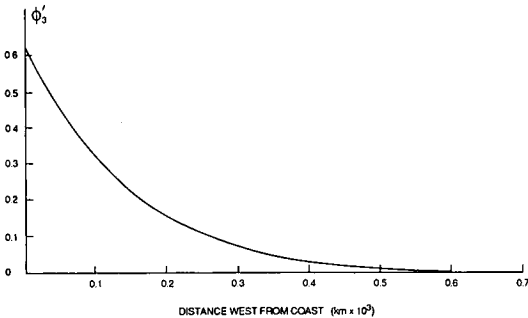
where Λ is a positive constant and x is measured positive eastwards from the trough line.

Using this assumption, a solution can be found for ϕ_3' and is given by Eqn 31.

$$\begin{aligned} \phi_3' = G & \left[\frac{\ln x}{r q \gamma^2} + \frac{\exp(rx)}{r(r-q)(r^2 + \gamma^2)} \int \frac{\exp(-rx) dx}{x} \right. \\ & - \frac{\exp(qx)}{q(r-q)(q^2 + \gamma^2)} \int \frac{\exp(-qx) dx}{x} \\ & + \frac{1}{\gamma^2(r^2 + \gamma^2)(q^2 + \gamma^2)} \left[\left\{ \gamma(r+q) \sin \gamma x \right. \right. \\ & + (\gamma^2 - rq) \cos \gamma x \left. \right\} \int \frac{\cos \gamma x}{x} dx \\ & + \left. \left\{ (\gamma^2 - rq) \sin \gamma x - \gamma(r+q) \cos \gamma x \right\} \int \frac{\sin \gamma x}{x} dx \right] \dots 31 \end{aligned}$$

where G is a positive constant. ϕ_3' in this equation is the lower-layer geopotential perturbation produced solely by latent heat release.

Fig. 12 Zonal variation in the relative magnitude of lower-layer geopotential ϕ_3' at 20°S due to the release of latent heat (ϕ_3' scale is included only to display relative magnitudes).



The integrals in Eqn 31 may be determined by expanding the integrands as power series. Using the values of U_1, U_3, σ_2, C_D and P_3 for case 1, the form of ϕ_3' can be found. Figure 12 displays the variation of ϕ_3' along 20°S derived from Eqn 31.

Discussion of results

When only orography is taken into account, the model produces a feeble ridge along the highest topography and a weak lee trough (Fig. 3). This pattern is in agreement with arguments based upon the principle of conservation of potential vorticity. However, the weakness of the perturbations suggests that orographic effects play only a limited role in the formation of the inland trough.

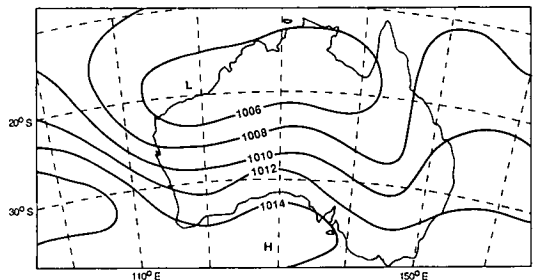
The incorporation of surface heating into the analysis results in trough/ridge systems bearing a close resemblance to actual mean summertime conditions. Figure 13 displays the mean sea level pressure contours over Australia for January. Compared to the case of orography alone, the model ridges have become much more marked and their axes have moved from the proximity of the highest topography to a position close to the coast. The inland troughs are roughly in the same positions as for orography alone but have deepened significantly.

The effect of vertical shear on the flow becomes apparent if a comparison of cases 1, 5 and 6 (Figs 4, 8 and 9) is made. Vertical shear acts as a damping mechanism on the perturbations in the flow. The amplitude of the perturbations decreases markedly as the vertical shear is increased; a result in agreement with the work of Rooney and Janowitz (1979) and Fandry and Leslie (1984).

Figures 4, 5 and 6 illustrate that as the depth of the low-level easterly stream is lessened (while the vertical shear between levels 1 and 3 is kept constant) the low-level flow becomes increasingly perturbed. The effect is significant and leads to very sharp troughs when the easterly winds are shallow (Fig. 6).

Changing the static stability parameter from $2 \times 10^{-4} m^3 k^{-1} (hPa)^{-1}$ to $3 \times 10^{-4} m^3 k^{-1} (hPa)^{-1}$ had a negligible effect on the easterly flow (compare cases 1 and 4, Figs 4 and 7). As the static stability is a function

Fig. 13 January mean sea level synoptic chart at 0000 UTC (from Taljaard et al. 1969).



of the lapse rate, the results indicate that the degree of atmospheric instability does not directly have much influence on the meteorological characteristics of northeastern Australia's inland trough. Any significant effect due to atmospheric instability would be indirect and linked to the atmosphere's potential to release latent heat in convection.

Figure 11 shows that a barely discernible stationary wave exists in the upper-level westerly flow due to the effects of orography and surface heating. The upper-level ridge overrides the low-level trough while the upper-trough lies above the low-level ridge. Fandry and Leslie (1984) obtained a similar result with their model.

The inclusion of latent heat release in the model is based on the assumptions mentioned in the text and has only been carried out qualitatively. Figure 12 shows that the release of latent heat acts in such a way as to emphasise the coastal ridge. Thus, it can be postulated that the release of heat in convective clouds effectively deepens and helps to maintain the inland trough. This, in turn, assists in the formation of more convective cloud and the latent heat released in this cloud helps preserve the inland trough.

Summary

A two-layer diagnostic model in which low-level easterly winds are capped by upper-level westerlies has been used to capture the salient features of the low-level trough/ridge system that prevails over northeastern Australia. The model produces a coastal ridge and a trough about 700 kilometres inland. The results obtained suggest that surface heating of the land mass is the most important factor in the formation of the trough. The Great Dividing Range exerts some influence on the low-level flow but this is of less importance than surface heating.

The trough frequently acts as a triggering mechanism for the formation of convective cloud in the moist air to its east. The release of latent heat in these clouds complements the effects of surface heating and orography. The latent heat released in convection, therefore, acts in a symbiotic fashion with orography and surface heating to maintain the inland

trough. The dry-line properties of the trough arise from the interaction between surface heating, orography and latent heat release.

The trough's features, determined by the model, show that it increases considerably in amplitude as the atmosphere becomes more barotropic and as the depth of the low-level easterly winds decreases. Altering the values of drag coefficient and mid-tropospheric static stability does not significantly influence the trough/ridge system.

The upper-level flow is much more zonal than the flow at low levels but also exhibits meanders due to orography and surface heating. The high-level trough is over the low-level ridge while the upper ridge lies above the low-level trough.

References

- Burkill, J. C. 1956. *The Theory of Ordinary Differential Equations*. Oliver and Boyd Ltd, Edinburgh, 102 pp.
- De Lisle, J. F. and Harper, J. F. 1961. A calculation of the effect of large-scale heat sources on southern hemisphere sub-tropical wind flow. *Tellus*, 13, 56-65.
- Derome, J. and Wiin-Nielsen, A. 1971. The response of a middle-latitude model atmosphere to forcing by topography and stationary heat sources. *Mon. Weath. Rev.*, 99, 564-76.
- Fandry, C. B. and Leslie, L. M. 1984. A two-layer quasi-geostrophic model of summer trough formation in the Australian subtropical easterlies. *J. Atmos. Sci.*, 41, 807-18.
- Leslie, L. M. 1980. Numerical modelling of the summer heat low over Australia. *Jnl appl. Met.*, 19, 381-7.
- Rooney, D. M. and Janowitz, G. S. 1979. Flow over the Rocky and Andes mountains. Application of an analytical model. *J. Atmos. Sci.*, 36, 549-58.
- Skinner, T. C. L. and Leslie, L. M. 1982. Predictability experiments with Australia's west coast summer trough. *Aust. Met. Mag.*, 30, 241-9.
- Smagorinsky, J. 1953. The dynamical influence of large-scale heat sources and sinks. *Q. Jl R. met. Soc.*, 79, 342-66.
- Taljaard, J. J., Van Loon, H., Crutcher, H. L. and Jenne, R. L. 1969. Climate of the upper air: Southern hemisphere. Vol. 1. Temperatures, dewpoints, and heights at selected pressure levels. *NAVAIR 50-10-55*, Chief Naval Operations, Washington D.C., 135 pp.
- Wiin-Nielsen, A. 1973. *Compendium of Meteorology for use by Class 1 and Class 2 Meteorological Personnel. Volume 1*. WMO, Geneva.